Cerebral Cortex Communications, 2021, **2**, 1–12

doi: 10.1093/texcom/tgab028
Original Article

ORIGINAL ARTICLE

Automatic Processing of Numerosity in Human Neocortex Evidenced by Occipital and Parietal Neuromagnetic Responses

Amandine Van Rinsveld[1], Vincent Wens[2,3], Mathieu Guillaume[1], Anthony Beuel[1], Wim Gevers[1], Xavier De Tiège[2,3] and Alain Content[1]

[1]Center for Research in Cognition and Neurosciences (CRCN), UNI – ULB Neuroscience Institute, Université libre de Bruxelles (ULB), Brussels 1050, Belgium, [2]Laboratoire de Cartographie fonctionnelle du Cerveau (LCFC), UNI – ULB Neuroscience Institute, Université libre de Bruxelles (ULB), Brussels 1070, Belgium and [3]Magnetoencephalography Unit, Department of Functional Neuroimaging, Service of Nuclear Medicine, CUB – Hôpital Erasme, Brussels 1070, Belgium

Address correspondence to Amandine Van Rinsveld, CRCN – Center for Research in Cognition and Neurosciences, UNI – ULB Neuroscience Institute, Université libre de Bruxelles (ULB), 50, av. F. Roosevelt, CP191, 1050 Bruxelles, Belgique. Email: am.vanrinsveld@gmail.com

Abstract

Humans and other animal species are endowed with the ability to sense, represent, and mentally manipulate the number of items in a set without needing to count them. One central hypothesis is that this ability relies on an automated functional system dedicated to numerosity, the perception of the discrete numerical magnitude of a set of items. This system has classically been associated with intraparietal regions, however accumulating evidence in favor of an early visual number sense calls into question the functional role of parietal regions in numerosity processing. Targeting specifically numerosity among other visual features in the earliest stages of processing requires high temporal and spatial resolution. We used frequency-tagged magnetoencephalography to investigate the early automatic processing of numerical magnitudes and measured the steady-state brain responses specifically evoked by numerical and other visual changes in the visual scene. The neuromagnetic responses showed implicit discrimination of numerosity, total occupied area, and convex hull. The source reconstruction corresponding to the implicit discrimination responses showed common and separate sources along the ventral and dorsal visual pathways. Occipital sources attested the perceptual salience of numerosity similarly to both other implicitly discriminable visual features. Crucially, we found parietal responses uniquely associated with numerosity discrimination, showing automatic processing of numerosity in the parietal cortex, even when not relevant to the task. Taken together, these results provide further insights into the functional roles of parietal and occipital regions in numerosity encoding along the visual hierarchy.

Key words: approximate number sense, frequency-tagging, magnetoencephalography, numerosity

Received: 20 March 2021; **Revised:** 20 March 2021; **Accepted:** 5 April 2021

Introduction

Posterior parietal cortex has been recurrently associated with the processing of numbers and numerical magnitudes, especially regions along the intraparietal sulcus (IPS). Numerical magnitude can be grasped under different formats (symbolic, i.e., 10, verbal, i.e., 10, or nonsymbolic, i.e., ●●●●●●●●●●). Dehaene et al. (2003) advanced the idea of a core representation of numerical magnitude in an abstract, modality-independent format located in the IPS, since corroborated by multiple neuroimaging evidence (e.g., Piazza et al. 2004; see Sokolowski et al. 2017 for a meta-analysis).

Verguts and Fias's (2004) modelized the encoding of numerosity as a general neural system that derives abstract numerical representation from sensory input as following: a first layer of neurons for sensory input detection, a second layer for input summation, and a last layer implementing number selection. Further evidence has highlighted a gradient of nonsymbolic numerical representations along the dorsal stream, quite similarly to the low- to high-level visual processing gradient along the ventral visual stream: The SPL and IPS regions would support the representation of numerosity and the number-selective coding and occipito-parietal cortex would act as a transition zone potentially supporting the summation coding (Roggeman et al. 2011). Within this occipito-parietal stream, multivariate pattern recognition analyses of blood oxygen level–dependent (BOLD) signal have identified an increasing decoding of numerosity peaking at parietal regions, supporting the functional role of these regions for the highest-level representation of numerosity (Eger et al. 2009; Bulthé et al. 2014). Further, ultrahigh-field functional magnetic resonance imaging (fMRI) allowed mapping numerosity coding in the parietal cortex with exquisite spatial details (Harvey et al. 2013, 2015).

A set of adaptation studies by Burr and Ross (2008) and Burr et al. (2017) led to the "visual number sense" hypothesis, which postulates the mechanism to process numerosity occurs direct and not indirectly through building upon other visual features. Accordingly, numerosity could be directly processed by the visual system because it exhibits adaptation properties similar to other primary visual features (e.g., color). In fact, other visual features are important to consider along numerosity processing because they also vehiculate magnitude information. Indeed, the numerosity of a set of objects is intrinsically linked to other non-numerical visual information related to continuous magnitude: the occupied area, the size of the items, etc. Some authors proposed a common mechanism for numerical and non-numerical magnitude processing supported by at least partially common neural bases (Walsh 2003; Bueti and Walsh 2009). The questions of the contribution of continuous magnitudes to numerosity processing and/or the commonality between the mechanisms underpinning the extraction of each by the sensory system remain difficult to address because distinguishing numerosity from other magnitudes is complicated from a methodological point of view.

Neuroimaging evidence supported occipital cortex involvement in numerosity extraction, opening the possibility of an early decoding of numerosity information in the visual hierarchy. An fMRI study using a numerosity judgment task showed that decoding performances of numerosity were above chance both in occipital and parietal regions but only the decoding accuracy in parietal regions could be linked to behavioral performances (Lasne et al. 2019). Another study, comparing numerosity and average size judgments that were intermixed in the same task, showed that attention direction toward the numerosity modulated the parietal regions but not the occipital regions (Castaldi et al. 2019). In a passive viewing fMRI study, Dewind et al. (2018) showed early visual cortex responds to numerosity changes that cannot be entirely explained by visual cues and could correspond to object normalization. This study reported decoding of numerosity only in early visual cortex but not in parietal regions. As they used a passive viewing paradigm, these authors proposed that the IPS could rather be involved in top-down attentional mechanisms linked to numerosity processing.

Electrophysiological evidence further supported that number processing may start very early in the visual hierarchy (Fornaciai et al. 2017). The role of the primary visual cortex for numerosity has been emphasized by electroencephalography (EEG) studies disclosing early neural sensitivity to numerosity (Park et al. 2015; Park 2018; Lucero et al. 2020). Frequency-tagging EEG is interesting in this context because it allows to measure steady-state evoked response synchronized at the frequency of visual presentation (Regan 1977). More specifically, steady-state visual responses evoked by both numerosity and some continuous visual features have demonstrated implicit discrimination of these features (Guillaume et al. 2018; Van Rinsveld et al. 2020). This approach distinguishes responses to different features based on their presentation frequency (Norcia et al. 2015), without the need to isolate them in the visual presentation, which is crucial because numerosity is intrinsically correlated with non-numerical, continuous magnitude parameters. However, the low spatial resolution of EEG did not allow clearly disentangling occipital and parietal activity, which is essential to further characterize the occipital/parietal functional dissociation in the processing of numerosity and non-numerical magnitudes along the visual pathways.

The current study used magnetoencephalography (MEG) to combine the exquisite temporal resolution necessary for high-frequency tagging with sufficient spatial resolution to enable source localization along the visual hierarchy. We tested the hypothesis that implicit discrimination of numerosity and continuous magnitudes occurs in the visual occipital cortices. We measured to what extent parietal sources contribute to implicit discrimination to test the attentional account of IPS role in numerosity extraction. This was achieved using the fast periodic visual stimulation paradigm illustrated in Figure 1. We presented arrays of dots that randomly varied in numerosity and continuous features. Similarly to oddball paradigms, one feature was held constant across standards but was varied deterministically at the rate of 1.25 Hz (deviant items, occurring every 8 items). The feature identified by deviant items was either numerosity (i.e., the number of dots) or a continuous magnitude (i.e., dot size, total area, dot density, and convex hull). Importantly, both standard and deviant stimuli within each block differed because only one feature was periodically fixed (e.g., numerosity), whereas all others randomly varied. We expected that frequency-tagging neuromagnetic responses would allow specifically discriminating the periodic features and locating the underlying neocortical sources.

Materials and Methods

Participants

Twenty-one healthy adults participated in this study. Volunteers suffering from, or with a history of, neurological or neuropsychological disorders, learning disability such as dyscalculia, or uncorrected visual impairment, were not included. We excluded 1 participant due to unusable structural MRI necessary for MEG

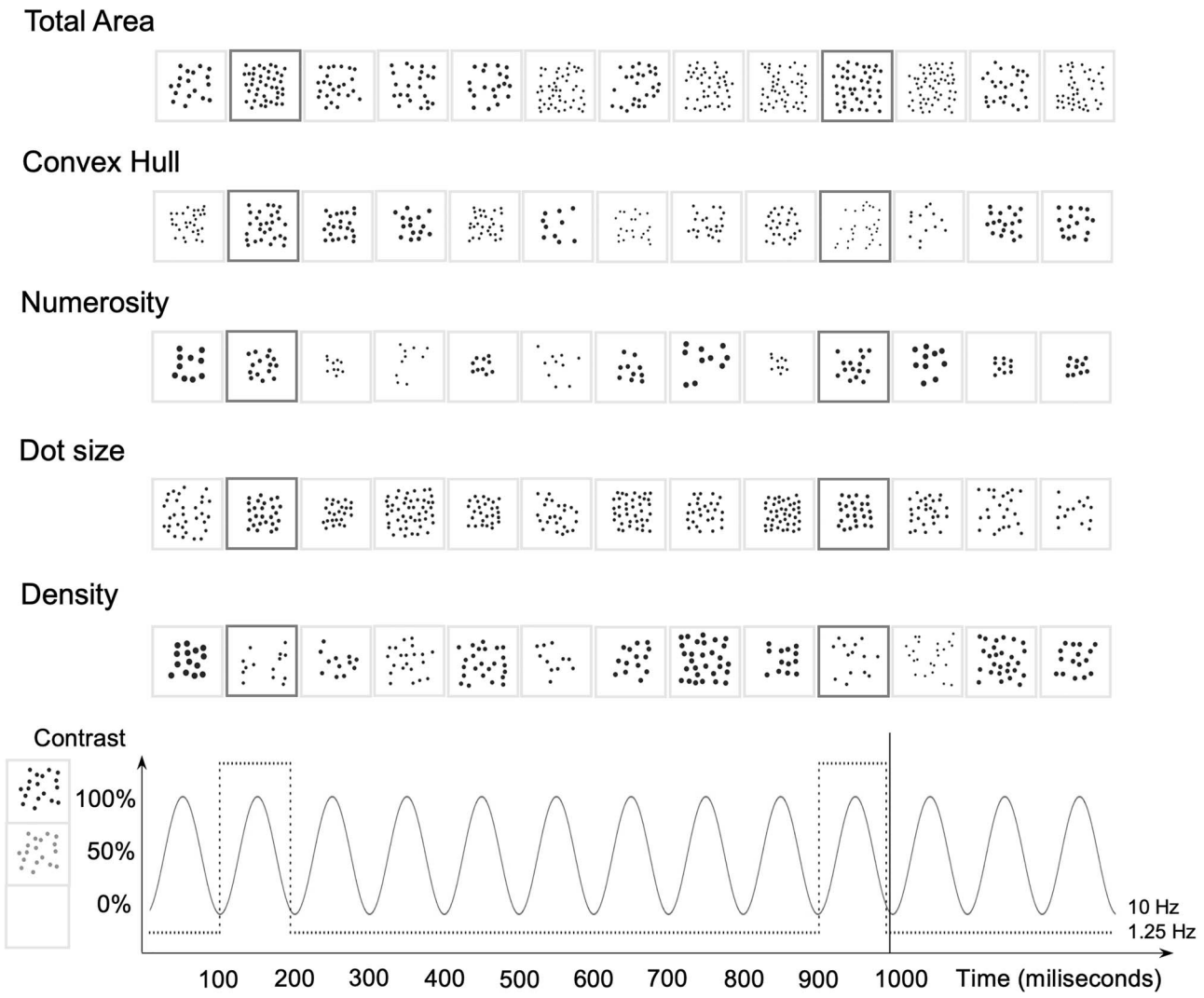

Figure 1. Sequences of dot patterns varying 5 features: dot size, total area, convex hull, density, and numerosity. Upper panels depict an example of 1.3-s long time series (13 stimuli) for the 5 experimental conditions. In each condition, the relevant feature is held constant across standard stimuli (light borders) and changed only in the deviant stimuli (dark borders) presented periodically, all other features being varied randomly. Ten stimuli are presented each second (10-Hz presentation rate), and deviants occur every 8 item (1.25-Hz oddball frequency). Each visual stimulus was presented with gradual contrast modulated sinusoidally at 10 Hz, as shown in the lower panel.

source localization. The final sample thus consisted of 20 participants, with a mean age of 23.5 years (range 20–29 years, 12 females). We followed APA ethical standards to conduct the study, which received prior approval by the CUB—Hôpital Erasme Ethics Committee (reference: P2018/362). The entire experiment lasted 3–4 h in total, and participants received 10€ per hour for their participation.

Visual Stimulation and Apparatus

Pictures showing dot arrays were generated with NASCO dot generation toolbox (Guillaume et al. 2020) as in previously validated EEG work (Van Rinsveld et al. 2020; for examples, see Fig. 1). We generated 100 standard pictures and 100 deviant pictures for each condition, each 850-by-850 pixel. Deviants were designed as standards except that the magnitude of one feature (total area, convex hull, numerosity, dot size, and density) was increased by a factor of 150%. Previous experimental parameter manipulations in SSVEPs with nonsymbolic material have demonstrated that the direction of the change did not impact the oddball frequency responses to numerosity changes (Kohler et al. 2020). Further evidence showed that this ratio is easily discriminated when adults perform magnitude judgment tasks (Barth 2003). From this database of pictures, we generated sequences of 440 stimuli made of series of 7 standards followed by one deviant. To avoid periodicity in the stochastic fluctuations in the nonrelevant features, we constructed the sequences so that all values taken by the nonrelevant features within deviant arrays appeared within standard arrays. A feature value that only appears within deviant trials can indeed elicit a periodic fluctuation since the probability of this value appearing is not evenly distributed across all trials. We thus made sure that no value was specific to the deviant trials (except for the target dimension). We then extracted the Fourier spectrum of the time series for each feature presentation and z-score normalized it. We only retained sequences in which the spectral z score of the feature of interest exceeded 2.32 (corresponding to the unilateral threshold at 99% of a standard normal

probability distribution) at 1.25-Hz deviant frequency, and concurrently the spectral z score of the other features was below this threshold. The sequence of each condition was repeated 4 times to increase the signal-to-noise ratio.

The fast periodic presentation of the stimuli was handled with the Psychophysics Toolbox (MATLAB, The MathWorks, Brainard 1997; Kleiner et al. 2007). Visual stimulation was displayed at 1 meter from the participants at the center of a MEG-compatible screen inside the magnetically shielded room (Maxshield, MEGIN), via a DLP projector (Panasonic PT-D7700E; 60-Hz refresh rate, 1366 × 768 pixels of resolution) placed outside the room and projection through a feedthrough.

Experimental Procedure

Participants were comfortably seated in the MEG armchair in front of the screen. They were instructed to look at the screen and to keep their gaze fixed on a diamond that was continuously displayed in blue at the center of the screen. Each time the fixation diamond changed color (red), participants had to press a key on a MEG-compatible response pad. Changes randomly occurred between 4 and 8 times in a sequence. This aimed at maintaining a similar vigilance level across conditions and refraining participants from looking away. Stimulus sequences were displayed with sinusoidal contrast modulation from 0% to 100% (Lochy et al. 2019; Fig. 1) at the base rate of 10 Hz (one stimulus presented every 100 ms), for a total duration of 44 s length. Five sequences were presented, in which one feature (total area, convex hull, numerosity, density, and dot size) was held fixed among standards and systematically changed in deviants, which occurred every 8 items (1.25 Hz oddball frequency). Two seconds of fade-in and 2 s of fade-out were added respectively at the beginning and at the end of each sequence to ensure smooth transition to the stimulations but were discarded from analyses. The order of the sequences was randomly counterbalanced across participants. At the end of the experiment, no participant reported noticing neither periodicity nor the feature of interest.

Data Acquisition

Visual evoked magnetic fields were measured using a whole-scalp-covering MEG system (Triux, MEGIN) containing 102 triplets of sensors, one magnetometer and 2 orthogonal planar gradiometers. Neuromagnetic activity was recorded continuously during each sequence, with internal active compensation (Maxshield, MEGIN), analog band-pass filtering between 0.1 and 330 Hz, and digital sampling at 1 kHz. The timing of sequence start and end (i.e., without fade-in and fade-out periods) was identified by a trigger signal. Four coils on the participants' head allowed to track head position continuously. Their location with respect to fiducials and over 300 scalp points sampling the head shape were obtained by 3-dimensional digitalization (Fastrak Polhemus). High-resolution structural 3D T1-weighted MRI of the participant's brain was acquired after the MEG session with a 1.5 T MRI scanner (Intera, Philips).

Data Processing

Environmental noise and head movements were corrected offline using signal space separation (Taulu et al. 2005) as implemented in the Maxfilter software (MEGIN, v2.2). Independent component analysis was then applied on the resulting MEG signals band-filtered between 0.5 and 45 Hz, to identify and suppress ocular and cardiac artifacts (Vigario et al. 2000). The cleaned data were chunked into four 44-s long epochs corresponding to the repetition of the same visual sequence and were averaged to increase signal-to-noise ratio (Liu-Shuang et al. 2014).

To enable the reconstruction of source activity underlying MEG data, we also processed the structural MRIs to compute individual forward models. MRI and MEG data were first co-registered manually using the digitized fiducial points for initial approximation and head-surface points for refinement (MRIlab, MEGIN). Forward modeling was then performed using the single-layer boundary element method implemented in the MNE-C suite (Gramfort et al. 2014), based on MRI segmentation obtained from the Freesurfer software (Fischl 2012). The forward model was computed for 3-dimensional sources located on the nodes of a volumetric brain grid, which was built from a regular 5-mm grid in the Montreal Neurological Institute (MNI) template MRI (16 102 nodes) and transformed into individual MRIs using a non-linear spatial normalization (Ashburner and Friston) implemented in the SPM12 toolbox (Friston et al. 2007).

Spectral Analysis

The Fourier coefficients of the averaged MEG data chunk were computed via discrete Fourier transformation of their first 40 s, leading to a frequency resolution of 0.025 Hz, and source projected by minimum norm estimation (MNE; Dale and Sereno 1993). The MNE projector was built from the individual forward model, noise covariance obtained from empty room MEG recordings, and a regularization parameter set via the prior consistency condition (Wens et al. 2015). Spectral amplitude was finally obtained at each source location as the Euclidean norm of the 3 components Fourier magnitudes.

Given our oddball paradigm, we focused on the detection of spectral peaks at the base (10 Hz) and oddball (1.25 Hz) frequencies and their harmonics. We extracted the amplitude spectra in frequency intervals centered on the frequency of interest and some harmonics (base frequency: 10 and 20 Hz; oddball: all multiples of 1.25 Hz smaller than 10 Hz) and summed them (sum-based amplitude, SBA). To assess the size of the peak at the target frequency, we compared the SBA for the target frequency bin to the SBA for neighboring bins (10 adjacent bins on both sides, the closest left and right neighbors being discarded). This comparison was carried out by standardizing the target SBA value, that is, by subtracting the mean SBA over neighbor bins and dividing by their standard deviation. This led to 2 brain maps of standardized SBA per participant, one corresponding to the base rate and the other to the oddball rate.

Statistical significance of these maps was assessed at the group level using unilateral parametric t tests against the null hypothesis that there was no difference. The significant threshold at $P = 0.05$ was $t_{19} = 1.725$. However as each map encompassed a large number (i.e., 16 102) of tests, a substantial number of false positives would be expected. The family-wise error rate was controlled by estimating the number of spatial degrees of freedom in MNE maps based on the forward model rank ($N = 62$ in this data, see Wens et al. 2015 for details) and applying Bonferroni correction, i.e., performing all univariate tests at $P < 0.05/N = 0.0008$). The resulting corrected threshold was $t_{19} = 3.632$.

To compare the conditions that showed significant oddball responses, we ran contrast analyses by subtracting conditions 2 by 2 and generating statistical maps assessing the significance of the difference at the group level using bilateral parametric

Table 1. Sources localization of the significant oddball responses for the 5 conditions

Condition	Peak localization	X	Y	Z	t	Voxels	Labels
Total area	Right primary visual cortex	30	−82	10	5.20	211	A
	Left intraparietal sulcus	−30	−72	60	4.45	5	B
Convex hull	Right lateral occipital	45	−77	15	7.39	514	A
	Right superior temporal gyrus	55	−62	20	4.23	28	B
	Left Fusiform gyrus	−25	−42	−15	4.05	9	C
Numerosity	Right supplementary motor area	15	−17	50	4.46	9	A
	Right intraparietal sulcus	30	−47	45	4.04	10	B
	Left precuneus	−10	−72	60	3.99	2	C
	Right cuneus	20	−87	45	3.97	4	D
	Right middle temporal gyrus	65	−52	10	3.93	2	E
Density	Right superior parietal lobule	15	−62	75	3.67	1	/
Dot size	No source above significance threshold						/

Note: X, Y, Z, t: MNI coordinates of the local maxima in the t maps, and the corresponding t_{19} value. Voxels: number of suprathreshold voxels in the connected cluster of the corresponding local maximum. Labels: provided for comparison with topographical maps shown in Figure 3.

t tests against the null hypothesis that all *t*s = 0. The significant threshold at $P = 0.05$ was $t_{19} = 2.086$, and the family-wise error corrected threshold was $t_{19} = 3.930$. These contrast maps are reported to visualize the discrepancies between conditions at the whole brain level but not to accurately localize the sources of these differences. Indeed, recent evidence demonstrated that MEG parametric contrast maps are suited to assess the existence of differences between conditions but not to draw conclusions about the source localization of these differences (Bourguignon et al. 2018). Analyses on non-contrast maps should be preferred to identify the sources of the observed differences. To overcome this limitation, we further ran repeated-measure analyses of variance to assess the differences of SBA between conditions in the sources that were the maximum of each condition as reported in Table 1. Analyses of variance (ANOVAs) were computed with JASP software (JASP 2018). Bonferroni–Holm corrections for multiple comparisons were applied for post-hoc comparisons between conditions.

Results

At the base rate of 10 Hz, SBA peaks were observed in all conditions, with maximal peak location in the medial occipital regions (map maximum $t = 10.73$, averaged over the 5 conditions) and were located in the occipital regions (Fig. 2). These steady-state responses at the base rate did not attest any discrimination of the feature of interest, as expected from our experimental design.

At the oddball rate (1.25 Hz), significant SBA peaks emerged clearly when modulating the magnitude of 3 features only: total area, convex hull, and numerosity, with different source locations (Fig. 3 and Table 1).

The sources of the oddball response to periodic changes in total area were located in bilateral medial occipital regions with a local maximum in the right primary visual cortex. A second source was located at the left IPS. Changes in convex hull identified bilateral medial occipital regions, with a local maximum at the right lateral occipital gyrus. A second source emerged at the right superior temporal gyrus, and a third more ventrally, along the left fusiform gyrus.

Changes in numerosity (i.e., the number of dots) disclosed right occipital and right temporal sources, as in the previous condition, and a source in the left precuneus. Two other close but distinct sources emerged, one in the right supplementary motor area and the other in the right IPS.

Density periodic modulations only identified a single-voxel suprathreshold source in the right superior parietal lobule, which is not visible on source maps because of smoothing. Finally, no significant peak was observed at the oddball frequency in response to the dot size condition.

To compare the level of synchronization on the oddball frequency between conditions, we ran repeated-measure ANOVAs with condition (3) as within-subject factor in each maximum peak identified from the previous analysis (Table 1). Statistical maps of the contrasts are presented in Figure 4 for visualization purposes and the results from the ANOVAs are summarized in Figure 5.

At the right primary visual cortex peak from the Total Area condition, we observed a marginal effect of condition, $F(2,38) = 2.537$, $P = 0.092$, $\eta^2 = 0.118$. Post-hoc comparisons showed that SBA of Total Area was larger than that of Numerosity, $t(19) = 2.157$, $P = 0.022$, whereas other post-hoc condition comparisons did not reach significance, $t(19) < 1$, $Ps > 0.2$. For both right occipital peaks for Convex Hull and Numerosity, no effect of condition was observed, $F(2,38) = 0.268$, $P > 0.2$, $\eta^2 = 0.014$ and $F(2,38) = 0.221$, $P > 0.2$, $\eta^2 = 0.012$.

Concerning central and parietal peaks, both the left precuneus maximum from Numerosity and the left IPS maximum from Total Area showed no effect of condition, $F(2,38) = 0.521$, $P > 0.2$, $\eta^2 = 0.027$ and $F(2,38) = 0.177$, $P > 0.2$, $\eta^2 = 0.009$. At the right supplementary motor area maximum from Numerosity, there was an effect of condition on the SBA, $F(2,38) = 6.118$, $P = 0.005$, $\eta^2 = 0.244$. Post-hoc comparisons revealed a larger SBA in Numerosity than in Total Area, $t(19) = -3.219$, $P = 0.014$, a marginal difference between Convex Hull and Total Area, $t(19) = -2.158$, $P = 0.087$, but no difference between Convex Hull and Numerosity, $t(19) = -1.412$, $P = 0.174$. Moreover, at the right IPS peak from Numerosity, there was a marginal effect of condition, $F(2,38) = 2.921$, $P = 0.066$, $\eta^2 = 0.133$. Post-hoc comparisons showed that Total Area and Numerosity differed significantly, $t(19) = -3.109$, $P = 0.017$, whereas other comparisons did not reach significance, $t(19) < 1$, $P > 0.2$.

In temporal regions, an effect of condition was observed at the left fusiform gyrus peak from Convex Hull, $F(2,38) = 4.950$, $P = 0.012$, $\eta^2 = 0.207$. Post-hoc comparisons showed a difference between Total Area and Convex Hull, $t(19) = -3.015$, $P = 0.021$ and between Convex hull and Numerosity, $t(19) = 2.761$, $P = 0.025$, but not between Total Area and Numerosity, $t(19) < 1$, $P > 0.2$. At the right superior temporal gyrus maximum from Convex Hull, there was no significant effect of conditions, F

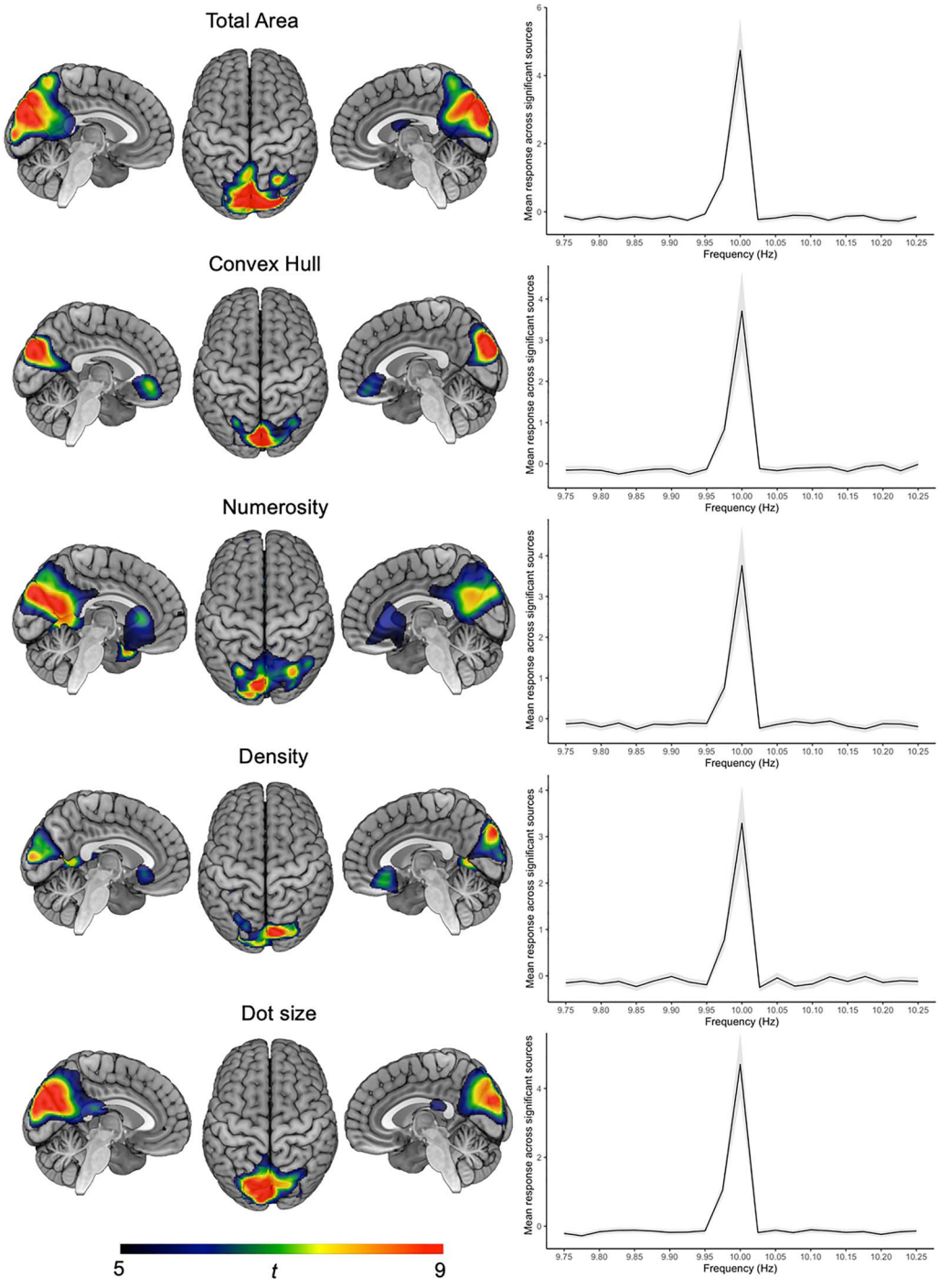

Figure 2. Statistical maps of standardized SBA at the base rate (i.e., 10 Hz) for the 5 conditions (total area, convex hull, numerosity, dot size, and density). The color scale corresponds to the statistical t_{19} values. Graphs represent the mean standardized SBA response across significant sources as a function of frequency. Gray ribbon depicts standard deviations across these sources.

(2,38) = 1.691, $P = 0.198$, $\eta^2 = 0.082$. At the right middle temporal gyrus maximum from Numerosity, the condition had a marginal effect, F (2,38) = 2.744, $P = 0.077$, $\eta^2 = 0.126$, though post-hoc comparisons did not show any significant differences (Total Area vs., Numerosity, $t(19) = -2.230$, $P = 0.114$, Convex Hull vs., Numerosity, $t(19) = -1.622$, $P > 0.2$, and Total Area vs., Convex Hull, $t(19) = -1.009$, $P > 0.2$).

In summary, the ANOVAs comparing the 3 conditions yielding significant oddball synchronization corroborate the differences pictured in the contrast maps. The occipital sources located in

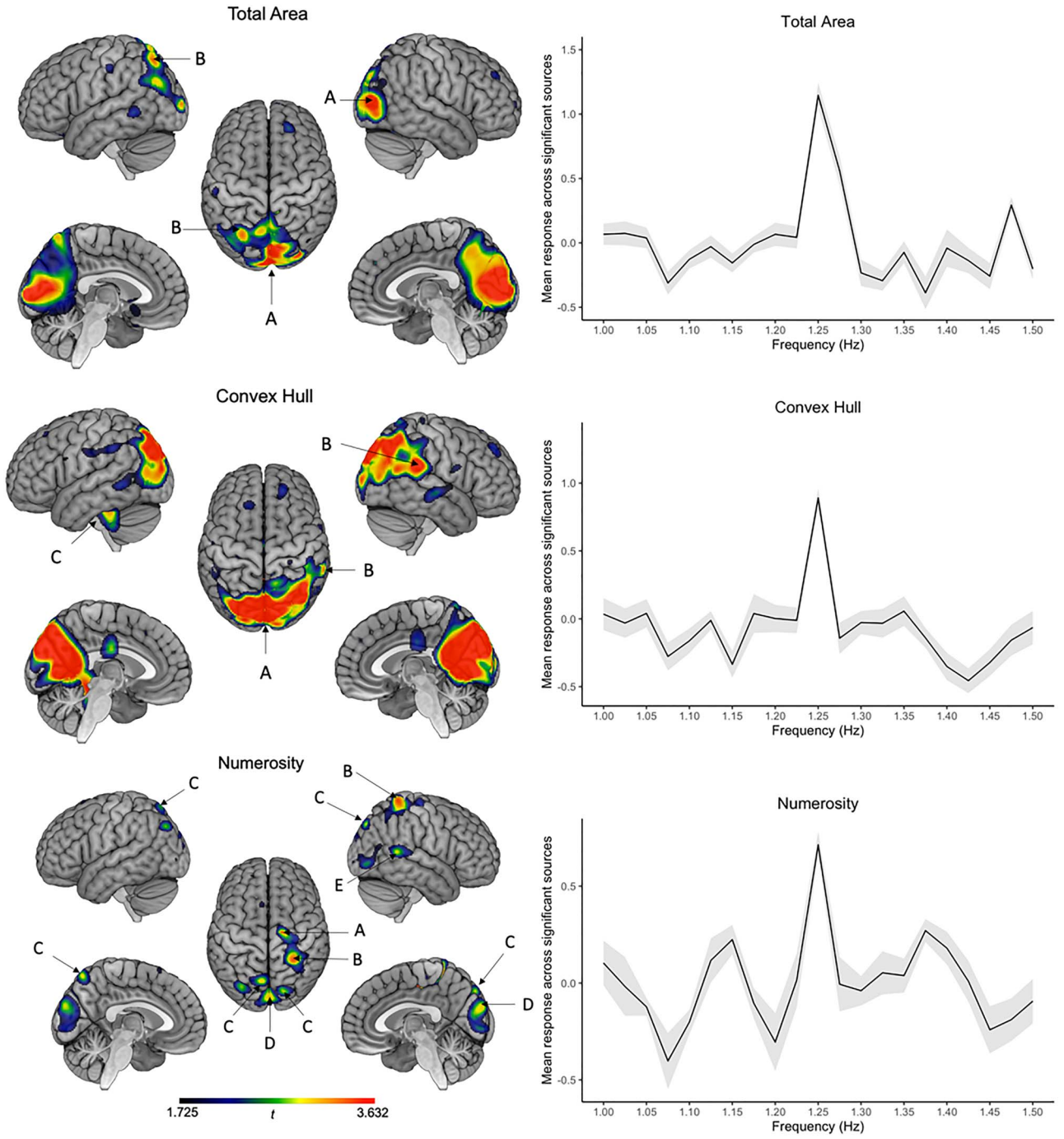

Figure 3. Statistical maps of standardized SBA at the 7 first harmonics of 1.25 Hz for the 3 conditions where significant periodic oddball responses were recorded (total area, convex hull, and numerosity). Color scale corresponds to t_{19} values: t(uncorrected) = 1.725, t(corrected) = 3.632. Labels correspond to distinct sources, as summarized in Table 1. Graphs represent the mean standardized SBA response across significant sources as a function of frequency (the 7 first harmonics of each frequency on the x axis were considered in the mean responses). Gray ribbon depicts standard deviations across these sources.

the lateral occipital and cuneus regions are relevant to the 3 conditions with a tendency toward a more stronger response of the primary visual cortex for the Total Area condition. Some of the parietal sources seem equivalent across conditions: left precuneus and IPS, while the right IPS and the right supplementary motor area are found only for Numerosity and Convex Hull with a tendency to a stronger response in Numerosity than in Convex Hull. Concerning the temporal regions, the fusiform gyrus response seems to be a specific of the Convex Hull condition as it is not found in the other conditions. Further right temporal gyrus sources were found both in Convex Hull and Numerosity but not in Total Area, although statistical comparisons between conditions in these regions were not significant.

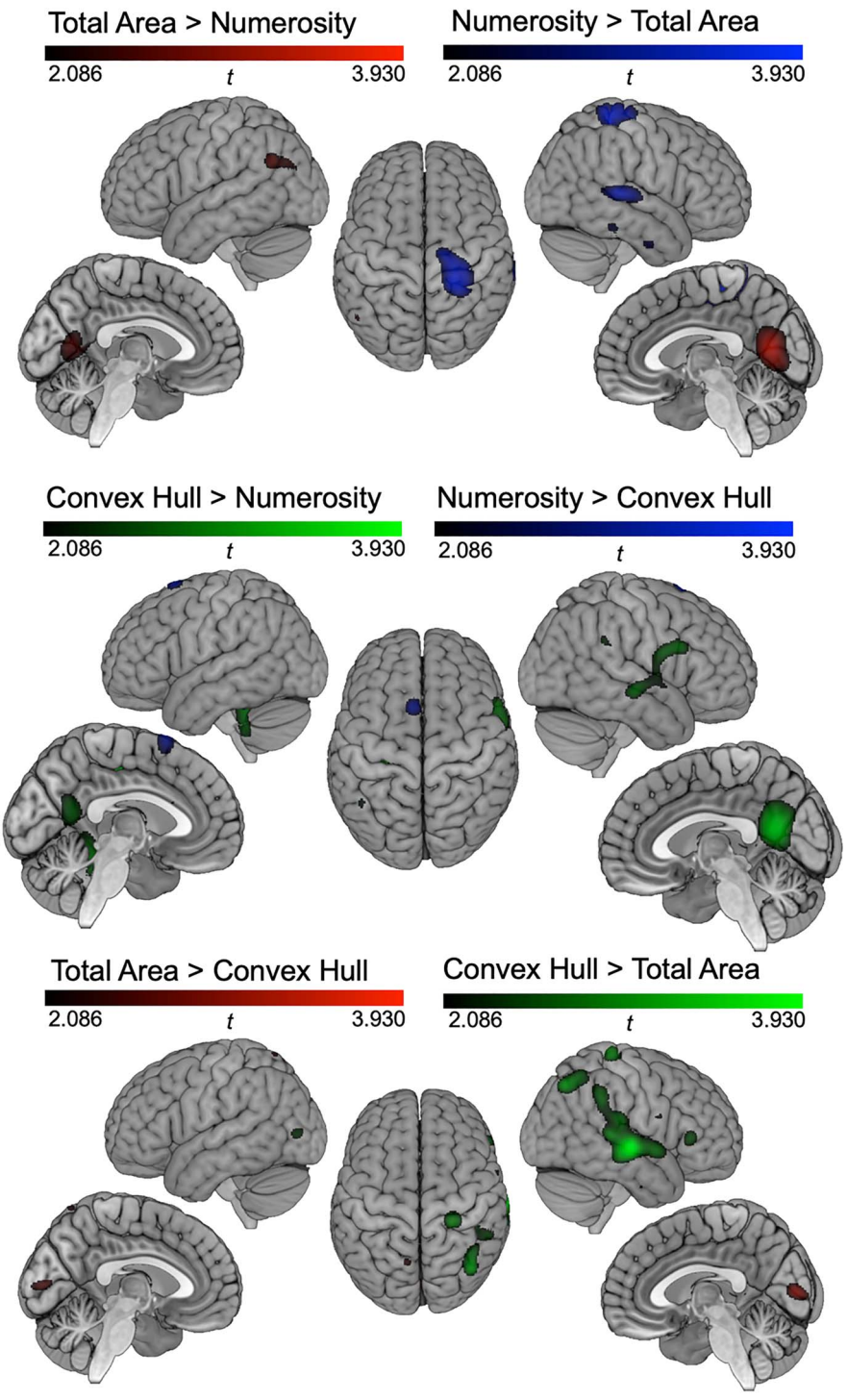

Figure 4. Statistical maps of the contrasts between the 3 conditions where significant periodic oddball responses were recorded (total area, convex hull, and numerosity). Color scale corresponds to t_{19} values: t(uncorrected) = 2.086, t(corrected) = 3.930.

Discussion

Extensive research has been dedicated to the neural basis of the ANS along the visual stream, but the earliest processing steps remain unclear. This is due to the difficulty to specifically target numerosity processing with high temporal and spatial resolution. For this reason, the current study used MEG to address the automatic processing of numerical and non-numerical magnitude along the visual hierarchy. Steady-state visual evoked neuromagnetic responses were measured to identify the neural correlates of the encoding of numerosity and of continuous magnitudes. Results showed significant frequency-tagged neural responses to the deviant Numerosity, Total Area and Convex Hull.

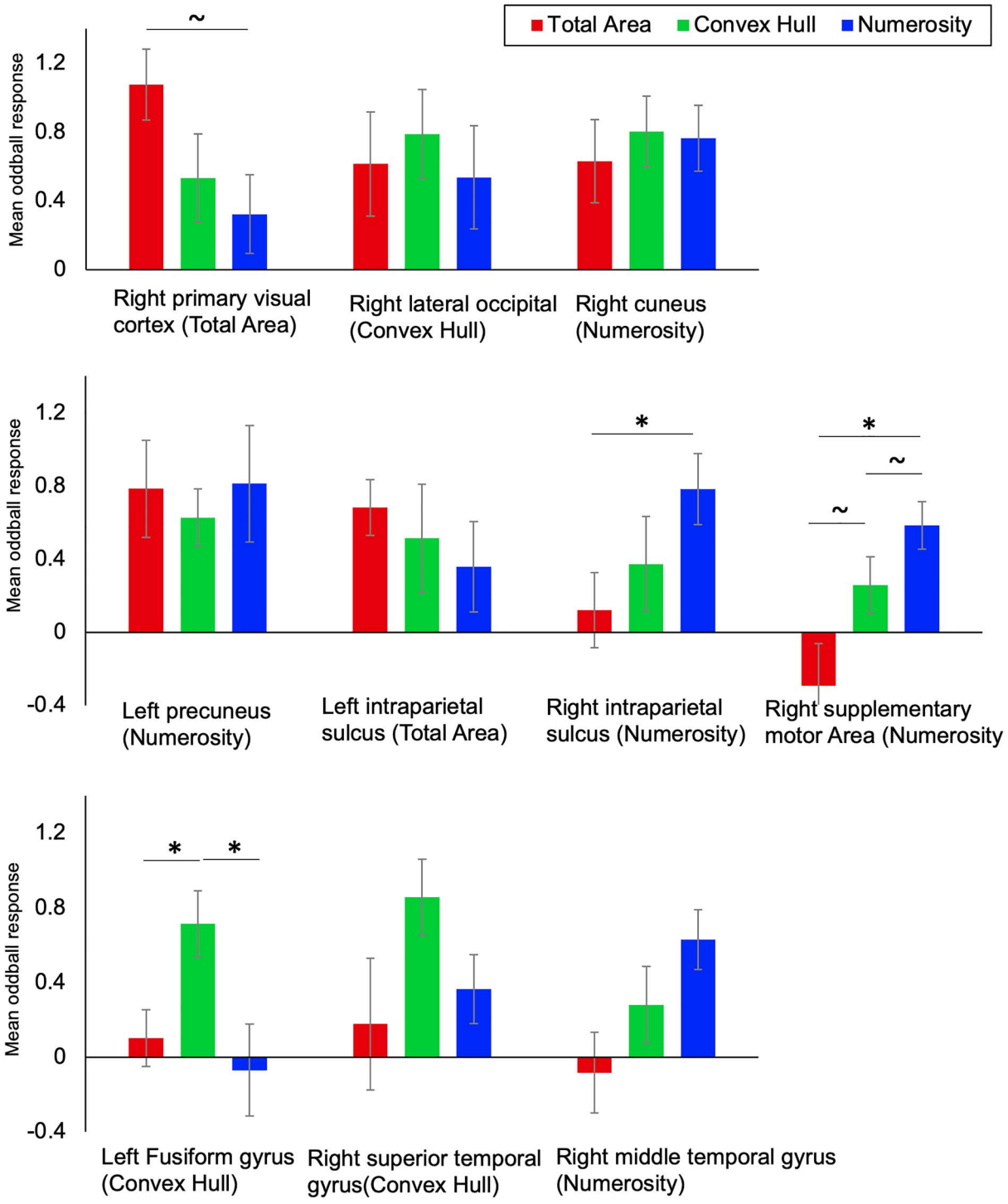

Figure 5. Mean SBA oddball responses as a function of the local maximum peaks from each condition. The condition in which each peak was identified as a maximum is mentioned under brackets. Color categories depict the SBA at the oddball rate for the Total Area (red), Convex Hull (green), and Numerosity (red) conditions. The upper, middle, and lower graphs gather together sources located respectively in occipital, in parietal and frontal, and in temporal regions. Significant differences between conditions are marked by a star. Error bars represent standard errors from the means.

Source reconstruction highlighted the respective involvement of common and distinct regions in implicit discrimination of numerical and continuous magnitude. Primary visual cortex was the most prevalent source for total area, whereas further parietal and temporal regions were more crucial in numerosity and convex hull encoding, respectively. Importantly, the right IPS was especially relevant to numerosity extraction even in an implicit discrimination requiring no explicit task attracting attention on any of the visual parameters of the stimuli.

These results thus show the robustness of implicit discrimination of numerosity, total areal and convex hull in MEG, as exactly those 3 dimensions were reported in previous EEG studies

(Van Rinsveld et al. 2020). Crucially, the source reconstruction of the current study shows that steady-state responses to periodic changes of numerosity are generated by early visual regions, but also parietal regions and to a lesser extent by temporal regions. Steady-state responses to changes of total area and convex hull were generated by a combination of both similar regions and different regions compared with numerosity discrimination. Our results thus support the visual number sense hypothesis (Burr and Ross 2008), that is, the idea that numerosity can be processed as a primary visual feature similarly to color or luminance. Further, we provide support to an encoding of numerosity and of certain continuous magnitudes that would both occur early in the dorsal visual pathway as some sources of the recorded responses were located in occipital cortex for both numerical and non-numerical magnitudes.

In the literature both early visual cortex and parietal regions supporting numerosity processing have been reported, depending on the experimental paradigm and on the type of measures. Particularly, activation of parietal regions was reported to be modulated by attention to the numerosity (Castaldi et al. 2019). An fMRI metanalysis contrasted brain activations from studies using active discrimination tasks and passive viewing of nonsymbolic stimuli (Sokolowski et al. 2017): Passive designs still comprised brain activations covering the right precuneus, superior parietal lobule and middle occipital gyrus. A visuo-spatial account of these findings was proposed because the superior parietal lobule is specifically associated with visuo-attentional processing involved in nonsymbolic numerical tasks. The current study provides further evidence of parietal activity spreading to the supplementary motor area in absence of any explicit magnitude discrimination task and even in the absence of any conscious perception of the periodic changes (i.e., no participant reported noticing periodicity or dimension changes in any experimental condition). The medial part of the supplementary motor area has been functionally associated to supplementary eye field which would be responsible for preparation of eye movements in goal-directed behavior (Nachev et al. 2008). This activation was mainly associated to numerosity in the current study, which further supports the dorsal visual system sensitivity to change in number.

Posterior parietal regions comprise several nodes of the dorsal attention network. Specifically, intraparietal regions are typically associated to spatial attention (Silver and Kastner 2009). These regions receive visual input from the primary visual areas but also through the superior colliculus route, and they may influence the activity of primary visual regions in return. Further studies will need to address the directionality of those activations that the current experimental design does not allow to distinguish. Attention orientation can be segregated in 2 distinct mechanisms: exogenous orienting of attention that is the involuntary orientation toward a salient stimulus due to the stimulus itself (bottom-up), and endogenous stimulus-driven attention where attention is reoriented to a stimulus that is relevant to a particular task (top-down; Bisley et al. 2011; Chica et al. 2013). The neuromagnetic responses to the fast periodic stimulation used in the current study are likely to be driven by the former involuntary attentional mechanisms but do not preclude that in magnitude judgment tasks that have been used extensively across the literature, a mixture of both types of orientation of attention co-exists and interact. Indeed, IPS, IPL, and SPL activity are modulated by the endogenous visuospatial attention and leading to reorientation of attention adapted to the demand of the task (Kastner et al. 1999; Corbetta et al. 2000). Previous evidence showed that posterior parietal cortex is involved both in conscious and nonconscious processing of visual stimuli (Kravitz et al. 2011) and this is probably the case for numerosity processing, nuancing the pure top-down attentional account previously proposed for parietal regions' function in numerical cognition (Dewind et al. 2018).

Moreover, we also observed a temporal source for the Convex Hull condition along the fusiform gyrus that was not present in both other conditions. This region is usually associated to the ventral stream of object recognition and in this case could contribute to the automatic discrimination of the changes in the object shape (Martin 2007; Liu et al. 2008). Indeed, considering the collection of dots holistically as a whole object in itself, its convex hull delimits the shape occupied by this object in the visual scene (Watson et al. 2014). Taken together, we thus provide evidence in favor of an automatic processing of numerosity and continuous magnitude, even without paying attention to the dimensions spread across the visual pathways.

The observed source discrepancies between the 3 conditions yielding implicit discrimination responses have implications for the theoretical model of an "approximate number system," that is, a distinct functional system for numerosity encoding that is specific for numerosity and does not generalize to all kind of magnitude extraction (Dehaene et al. 2003; Walsh 2003). Previous evidence in favor of ANS were not reflecting a pure distinction between numerosity and continuous magnitude extraction because of the strong correlations between both and were complicated by the fact that processing both types of magnitude might partially share a common neural basis (Bueti and Walsh 2009). Although there are some commonalities between the 3 conditions showing that some steps may be similar, also major discrepancies emerged in the sources generating the implicit discrimination responses. The current results thus attest the involvement of a pattern of brain responses that is specific to involuntary numerosity processing and that is functionally distinct from a general system that would process all kind of magnitude similarly.

Concerning the neural mechanism of numerosity encoding, the current data support an early summation process that could occur both in parietal and occipital cortex and interestingly not only for numerosity but also for continuous magnitude. Crucially, the implicit discriminations observed here could not be performed based on the location of the dots or other parameters as the design ensured random variation of other parameters across the standard and deviant stimuli presented in the sequences. Some authors argued in favor of a summation coding of numerosity in the parietal regions that would be related to the spatial disposition of the dots in the visual scene (Cavdaroglu and Knops 2019). Their claim is based on evidence that decoding of numerosity from activation patterns in those regions is only observed for simultaneous presentation of the dot arrays in a comparison task, by opposition to sequential presentations of dot arrays where numerosity could be only decoded from occipital regions along the calcarine sulcus. In contrast, the current study encompassed both parietal and occipital sources related to the discrimination of numerosity, though we only used sequential presentations. Our results thus support the existence of a dedicated coding for numerosity both in parietal and occipital regions even in case of sequential presentation of the stimuli. This corroborates evidence of a functional dissociation between magnitude and spatial coding of numerosity among the intraparietal regions (Kanayet et al. 2018), showing that neither numerosity nor continuous magnitude coding can be reduced to sole spatial coding.

The implicit discrimination of magnitudes observed through the frequency-tagged responses generated by both occipital and parietal regions suggests that the system processes automatically some features of the visual scene linked to the number of elements and other global magnitude features (Greene and Oliva 2009). We demonstrated here that these isolated features are salient even in a task-irrelevant context. Crucially, the system also involuntary keeps track of those features across time ensuring that the next stimuli processing will take into account some characteristics of its predecessors. These results could thus be framed in the larger scope of the predictive coding theory which states that the mind is organized hierarchically to minimize prediction error with a constant feedback from other regions that adjusts the predictions in order to make optimal inferences about the environment (Friston 2008; Ester et al. 2016). The current study suggests that the dorsal visual stream can handle an efficient general description of the scene combining very early decoding of numerical and continuous magnitude information with a dynamic adjustment of perceptual experience.

In conclusion, the early visual regions would be able to discriminate numerosity and some of the continuous magnitudes (total area and convex hull) and the parietal regions may support the persistence of the information over short timescales. The frequency-tagged neuromagnetic responses provide evidence in favor of an automatic feature-based attention spontaneously directed toward numerosity and some continuous magnitude properties related to the whole visual scene. Crucially the experimental design ensured that the observed discrimination responses were invariant both to spatial disposition of the dots and to the intrinsic correlations among these dimensions because of the strict control of the visual stimulation.

Funding

European Union's Horizon 2020 research and innovation program under the Marie Skłodowska-Curie (grant agreement no. 799171 to A.V.); PDR project No T.1052.15 of Fonds National de la Recherche Scientifique to A.C. and W.G.

Notes

Conflict of Interest: The authors declare no conflict of interest that might be interpreted as influencing the research, and APA ethical standards were followed in the conduct of this work.

References

Ashburner J, Friston KJ. s. d. Nonlinear spatial normalization using basis functions. **13**.

Barth H. 2003. The construction of large number representations in adults. *Cognition*. **86**(3):201–221. doi: 10.1016/S0010-0277(02)00178-6.

Bisley JW, Mirpour K, Arcizet F, Ong WS. 2011. The role of the lateral intraparietal area in orienting attention and its implications for visual search: role of LIP in attention and visual search. *Eur J Neurosci*. **33**(11):1982–1990. doi: 10.1111/j.1460-9568.2011.07700.x.

Bourguignon M, Molinaro N, Wens V. 2018. Contrasting functional imaging parametric maps: the mislocation problem and alternative solutions. *Neuroimage*. **169**:200–211. doi: 10.1016/j.neuroimage.2017.12.033.

Brainard DH. 1997. The psychophysics toolbox. *Spat Vis*. **10**(4):433–436.

Bueti D, Walsh V. 2009. The parietal cortex and the representation of time, space, number and other magnitudes. *Philos Trans R Soc B*. **364**(1525):1831–1840. doi: 10.1098/rstb.2009.0028.

Bulthé J, De Smedt B, Op de Beeck HP. 2014. Format-dependent representations of symbolic and non-symbolic numbers in the human cortex as revealed by multi-voxel pattern analyses. *Neuroimage*. **87**:311–322. doi: 10.1016/j.neuroimage.2013.10.049.

Burr DC, Anobile G, Arrighi R. 2017. Psychophysical evidence for the number sense. *Philos Trans R Soc B*. **373**(1740):20170045. doi: 10.1098/rstb.2017.0045.

Burr D, Ross J. 2008. A visual sense of number. *Curr Biol*. **18**(6):425–428. doi: 10.1016/j.cub.2008.02.052.

Castaldi E, Piazza M, Dehaene S, Vignaud A, Eger E. 2019. Attentional amplification of neural codes for number independent of other quantities along the dorsal visual stream. *Elife*. **8**:e45160.

Cavdaroglu S, Knops A. 2019. Evidence for a posterior parietal cortex contribution to spatial but not temporal numerosity perception. *Cereb Cortex*. **29**(7):2965–2977. doi: 10.1093/cercor/bhy163.

Chica AB, Bartolomeo P, Lupiáñez J. 2013. Two cognitive and neural systems for endogenous and exogenous spatial attention. *Behav Brain Res*. **237**:107–123. doi: 10.1016/j.bbr.2012.09.027.

Corbetta M, Kincade JM, Ollinger JM, McAvoy MP, Shulman GL. 2000. Voluntary orienting is dissociated from target detection in human posterior parietal cortex. *Nat Neurosci*. **3**(3):292–297. doi: 10.1038/73009.

Dale A, Sereno M. 1993. Improved localization of cortical activity by combining EEG and MEG with MRI cortical surface reconstruction. *J Cogn Neurosci*. **20**.

Dehaene S, Piazza M, Pinel P, Cohen L. 2003. Three parietal circuits for number processing. *Cogn Neuropsychol*. **20**(3–6):487–506.

DeWind NK, Park J, Woldorff MG, Brannon EM. 2018. Numerical encoding in early visual cortex. *Cortex*. **114**:76–89.

Eger E, Michel V, Thirion B, Amadon A, Dehaene S, Kleinschmidt A. 2009. Deciphering cortical number coding from human brain activity patterns. *Curr Biol*. **19**(19):1608–1615. doi: 10.1016/j.cub.2009.08.047.

Ester EF, Sutterer DW, Serences JT, Awh E. 2016. Feature-selective attentional modulations in human frontoparietal cortex. *J Neurosci*. **36**(31):8188–8199. doi: 10.1523/JNEUROSCI.3935-15.2016.

Fischl B. 2012. FreeSurfer. *Neuroimage*. **62**(2):774–781. doi: 10.1016/j.neuroimage.2012.01.021.

Fornaciai M, Brannon EM, Woldorff MG, Park J. 2017. Numerosity processing in early visual cortex. *Neuroimage*. **157**:429–438. doi: 10.1016/j.neuroimage.2017.05.069.

Friston K. 2008. Hierarchical models in the brain. *PLoS Comput Biol*. **4**(11):e1000211.

Friston K, Ashburner J, Kiebel S, Nichols T, Penny W. 2007. *Statistical parametric mapping: the analysis of functional brain images*. Academic Press.

Gramfort A, Luessi M, Larson E, Engemann DA, Strohmeier D, Brodbeck C, Parkkonen L, Hämäläinen MS. 2014. MNE software for processing MEG and EEG data. *Neuroimage*. **86**:446–460. doi: 10.1016/j.neuroimage.2013.10.027.

Greene M, Oliva A. 2009. Recognition of natural scenes from global properties: seeing the forest without representing the trees. *Cogn Psychol*. **58**(2):137–176. doi: 10.1016/j.cogpsych.2008.06.001.

Guillaume M, Mejias S, Rossion B, Dzhelyova M, Schiltz C. 2018. A rapid, objective and implicit measure of visual quantity discrimination. *Neuropsychologia*. **111**:180–189. doi: 10.1016/j.neuropsychologia.2018.01.044.

Guillaume M, Schiltz C, Van Rinsveld A. 2020. NASCO: A new method and program to generate dot arrays for non-symbolic number comparison tasks. *J Numer Cognit*. **6**(1):129–147. doi: 10.5964/jnc.v6i1.231.

Harvey BM, Fracasso A, Petridou N, Dumoulin SO. 2015. Topographic representations of object size and relationships with numerosity reveal generalized quantity processing in human parietal cortex. *Proc Natl Acad Sci*. **112**(44):13525–13530. doi: 10.1073/pnas.1515414112.

Harvey BM, Klein BP, Petridou N, Dumoulin SO. 2013. Topographic representation of numerosity in the human parietal cortex. *Science*. **341**(6150):1123–1126. doi: 10.1126/science.1239052.

JASP Team. 2018. *JASP Version 0.9 Computer Software*. https://jasp-stats.org/.

Kanayet FJ, Mattarella-Micke A, Kohler PJ, Norcia AM, McCandliss BD, McClelland JL. 2018. Distinct representations of magnitude and spatial position within parietal cortex during number–space mapping. *J Cogn Neurosci*. **30**(2):200–218. doi: 10.1162/jocn_a_01199.

Kastner S, Pinsk MA, De Weerd P, Desimone R, Ungerleider LG. 1999. Increased activity in human visual cortex during directed attention in the absence of visual stimulation. *Neuron*. **22**(4):751–761. doi: 10.1016/S0896-6273(00)80734-5.

Kleiner M, Brainard D, Pelli D, Ingling A, Murray R, Broussard C. 2007. What's new in Psychtoolbox-3? *Perception*. **36**(14): 1–16.

Kohler PJ, Barzegaran E, Norcia AM, McCandliss BD. 2020. Parietal contributions to abstract numerosity measured with steady state visual evoked potentials [Preprint]. *Neuroscience*. doi: 10.1101/2020.08.06.239889 August 06, 2020, preprint: not peer reviewed.

Kravitz DJ, Saleem KS, Baker CI, Mishkin M. 2011. A new neural framework for visuospatial processing. *Nat Rev Neurosci*. **12**(4):217–230. doi: 10.1038/nrn3008.

Lasne G, Piazza M, Dehaene S, Kleinschmidt A, Eger E. 2019. Discriminability of numerosity-evoked fMRI activity patterns in human intra-parietal cortex reflects behavioral numerical acuity. *Cortex*. **114**:90–101.

Liu-Shuang J, Norcia AM, Rossion B. 2014. An objective index of individual face discrimination in the right occipito-temporal cortex by means of fast periodic oddball stimulation. *Neuropsychologia*. **52**:57–72. doi: 10.1016/j.neuropsychologia.2013.10.022.

Liu X, Steinmetz NA, Farley AB, Smith CD, Joseph JE. 2008. Midfusiform activation during object discrimination reflects the process of differentiating structural descriptions. *J Cogn Neurosci*. **20**(9):1711–1726. doi: 10.1162/jocn.2008.20116.

Lochy, A, de Heering, A, Rossion, B. 2019. The non-linear development of the right hemispheric specialization for human face perception. *Neuropsychologia*. **126**:10–19.

Lucero C, Brookshire G, Sava-Segal C, Bottini R, Goldin-Meadow S, Vogel EK, Casasanto D. 2020. Unconscious number discrimination in the human visual system. *Cereb Cortex*. **30**(11):5821–5829. doi: 10.1093/cercor/bhaa155.

Martin A. 2007. The representation of object concepts in the brain. *Annu Rev Psychol*. **58**(1):25–45. doi: 10.1146/annurev.psych.57.102904.190143.

Nachev P, Kennard C, Husain M. 2008. Functional role of the supplementary and pre-supplementary motor areas. *Nat Rev Neurosci*. **9**(11):856–869. doi: 10.1038/nrn2478.

Norcia AM, Appelbaum LG, Ales JM, Cottereau BR, Rossion B. 2015. The steady-state visual evoked potential in vision research: A review. *J Vis*. **15**(6):4. doi: 10.1167/15.6.4.

Park J. 2018. A neural basis for the visual sense of number and its development: A steady-state visual evoked potential study in children and adults. *Dev Cogn Neurosci*. **30**:333–343.

Park J, DeWind NK, Woldorff MG, Brannon EM. 2015. Rapid and direct encoding of numerosity in the visual stream. *Cereb Cortex*. bhv017. doi: 10.1093/cercor/bhv017.

Piazza M, Izard V, Pinel P, Le Bihan D, Dehaene S. 2004. Tuning curves for approximate numerosity in the human intraparietal sulcus. *Neuron*. **44**(3):547–555.

Regan D. 1977. Steady-state evoked potentials. *J Opt Soc Am*. **67**(11):1475.

Roggeman C, Santens S, Fias W, Verguts T. 2011. Stages of nonsymbolic number processing in occipitoparietal cortex disentangled by fMRI adaptation. *J Neurosci*. **31**(19):7168–7173. doi: 10.1523/JNEUROSCI.4503-10.2011.

Silver MA, Kastner S. 2009. Topographic maps in human frontal and parietal cortex. *Trends Cogn Sci*. **13**(11):488–495. doi: 10.1016/j.tics.2009.08.005.

Sokolowski HM, Fias W, Mousa A, Ansari D. 2017. Common and distinct brain regions in both parietal and frontal cortex support symbolic and nonsymbolic number processing in humans: a functional neuroimaging meta-analysis. *Neuroimage*. **146**:376–394. doi: 10.1016/j.neuroimage.2016.10.028.

Taulu S, Simola J, Kajola M. 2005. Applications of the signal space separation method. *IEEE Trans Signal Process*. **53**: 3359–3372.

Van Rinsveld A, Guillaume M, Kohler PJ, Schiltz C, Gevers W, Content A. 2020. The neural signature of numerosity by separating numerical and continuous magnitude extraction in visual cortex with frequency-tagged EEG. *Proc Natl Acad Sci*. **117**(11):5726–5732.

Verguts T, Fias W. 2004. Representation of number in animals and humans: a neural model. *J Cogn Neurosci*. **16**(9):1493–1504. doi: 10.1162/0898929042568497.

Vigario R, Sarela J, Jousmiki V, Hamalainen M, Oja E. 2000. Independent component approach to the analysis of EEG and MEG recordings. *IEEE Trans Biomed Eng*. **47**(5):589–593. doi: 10.1109/10.841330.

Walsh V. 2003. A theory of magnitude: Common cortical metrics of time, space and quantity. *Trends Cogn Sci*. **7**(11):483–488. doi: 10.1016/j.tics.2003.09.002.

Watson DM, Hartley T, Andrews TJ. 2014. Patterns of response to visual scenes are linked to the low-level properties of the image. *Neuroimage*. **99**:402–410. doi: 10.1016/j.neuroimage.2014.05.045.

Wens V, Marty B, Mary A, Bourguignon M, Op de Beeck M, Goldman S, Van Bogaert P, Peigneux P, De Tiège X. 2015. A geometric correction scheme for spatial leakage effects in MEG/EEG seed-based functional connectivity mapping: Spatial Leakage Geometric Correction Scheme. *Hum Brain Mapp*. **36**(11):4604–4621. doi: 10.1002/hbm.22943.